2018 IEEE International Conference on Robotics and Automation (ICRA)
May 21-25, 2018, Brisbane, Australia

Design and Analysis of a Fixed-Wing Unmanned Aerial-Aquatic Vehicle

Joseph Moore[1], Andrew Fein[2], and William Setzler[3]

Abstract— **In this paper, we describe the design and analysis of a fixed-wing unmanned aerial-aquatic vehicle. Inspired by prior work in aerobatic post-stall maneuvers for fixed-wing vehicles [1], we explore the feasibility of executing a water-to-air transition with a fixed-wing vehicle using almost entirely commercial off-the-shelf components (excluding the fuselage). To do this, we first propose a conceptual design based on observations about the dominant forces and dimensionless analysis. We then further refine this concept by building a design tool based on simplified models to explore the design space. To verify the results of the design tool, we use a higher fidelity model along with a direct hybrid trajectory optimization approach to show via numerical simulation that the water-to-air transition is feasible. Finally, we successfully test our design experimentally by hand-piloting a prototype vehicle through the water-to-air transition and discuss our approach for replacing the human-pilot with closed-loop control.**

I. INTRODUCTION

In the last few years, there has been a renewed interest in developing hybrid unmanned aerial-aquatic vehicles or UAAVs [2]. Although manned aerial-aquatic systems have been explored in the past [3], continued advances in technology associated with small to medium-sized air and water vehicles have provided an opportunity to develop novel *unmanned* vehicles that span both domains. These vehicles have the potential to enable new remote sensing and/or sampling operations where a single vehicle must access both aerial and aquatic environments. In addition, a hybrid aerial-aquatic provides a distinct advantage over underwater vehicles, since the UAAV can transition into the air domain to reduce drag when high speed travel is required.

In particular, we believe that *fixed-wing* aerial-aquatic vehicles have the potential to provide far greater efficiency and endurance than their rotorcraft counterparts, since, in steady state, most of the input power is used to overcome drag rather than generate lift. A combination of airfoil design and angle-of-attack can be used to more efficiently offset static forces such as gravity and buoyancy. Furthermore, for fixed-wing vehicles, the buoyancy of the fuselage in water can be used to assist in the water-exit, reducing the amount of power required to make the domain transition.

*This work was supported by the Johns Hopkins University Applied Physics Lab Internal Research and Development Program

[1]Joseph Moore is is a Research Scientist in the Intelligent Systems Group, Johns Hopkins University Applied Physics Lab, Laurel, MD, 20723 joseph.moore@jhuapl.edu

[2]Andrew Fein is a student in the Mechanical Engineering Department, University of Maryland, College Park, 20742 afein10@gmail.com

[3]William Setzler is a member of the Technical Support Staff in the Advanced Mechanical Fabrication Group, Johns Hopkins University Applied Physics Lab, Laurel, MD, 20723 william.setzler@jhuapl.edu

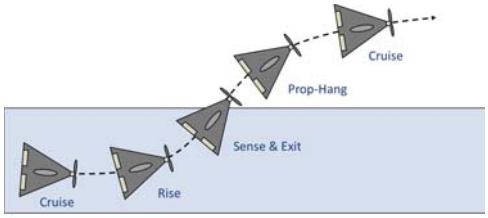

Fig. 1: A depiction of the fixed-wing UAAV executing a water-exit maneuver.

One application for which a fixed-wing unmanned aerial-aquatic vehicle might be especially well suited is exploring a land-locked body of water at a distance. In this case, the energetics of the vehicle could be of particular importance if the vehicle is required to travel long distances at high altitudes before diving down into a body of water to collect data. Another use case could be sparsely sampling water-columns in a large body of water very quickly, as might be desired in environmental monitoring. Using a fixed-wing aerial-aquatic vehicle could greatly improve endurance, if the distances between points of interest are large.

In this paper, we propose a propeller-driven fixed-wing aerial-aquatic vehicle that builds up speed underwater, exploits buoyancy to navigate the air-water boundary, and makes uses of aerodynamic lift forces to execute a prop-hang maneuver before transitioning into forward flight. While this approach will ultimately rely heavily on closed-loop control to enable a robust and fully autonomous solution, equally as important is being able to ensure the existence of a *feasible* trajectory given the vehicle design characteristics.

To this end, we develop tools and algorithms for exploring the effect of vehicle design parameters on water-exit feasibility. We first propose a notional design, based on arguments from basic physics and dimensionless analysis. We then explore the parameter space of our notional design by building a "design tool" based entirely on closed-form solutions for various parts of the maneuver. To validate this approach, we formulate an optimal hybrid trajectory optimization problem and compare the results with the output of the design tool. Finally, we build a prototype of our system and demonstrate the water-to-air maneuver experimentally. While our initial prototype is hand-piloted, we discuss our closed-loop control strategy for making the system fully autonomous.

II. RELATED WORK

Unmanned aerial-aquatic vehicles have received considerable attention over the last few years. These aerial-aquatic vehicles largely have their origins in autonomous sea planes [4], [5] which can autonomously land and take off from the

water's surface. Following this work, an effort was made in [6] to explore the mechanical design concepts associated with a robotic flying fish. The authors launch a passive vehicle from underwater and measure the forces required to overcome drag and exit the water at a reasonable cruise velocity. They determined that for a 10m/s exit velocity, prohibitively high power densities are required.

Until very recently, few aerial-aquatic vehicles were able to both enter and exit the water. A number of efforts have focused on vehicles capable of executing a air-to-water transition. MIT Lincoln Labs developed a hybrid aerial-aquatic vehicle [7] inspired by the Gannet bird which was able to dive into the water, but not able to exit again. Similarly, the Naval Research Lab developed the Flying-Swimmer or "Flimmer" [8], a UAV capable of diving into the water and operating as a submarine thenceforth. On the extremely small scale, authors in [9] demonstrated that a insect-scaled flapping micro UAV was capable of flying in air, landing on the water surface, and transitioning to swimming.

Conversely, researchers have also attempted to solve the water-exit problem. In addition to Flimmer, the Naval Research Laboratory developed the XFC Sea Robin, a submarine launched unmanned aerial vehicle [10]. Recently, researchers have enabled vertical take-off-and-landing from the water's surface with an aquatic fixed-wing UAV via a novel passive mechanism [11].

To date, only a small number of researchers have developed prototype systems capable of water-exit and water-entry. This work was preceded by a number of attempts to model and control hybrid-aerial aquatic quadrotors in simulation [12], [13]. This work eventually found its way into a hardware prototype in [14], where the authors demonstrated a very similar concept experimentally. Another vehicle capable of executing water-exit and water-entry can be found in [15], [16]. This vehicle has a unique approach for solving the water exit problem - it uses a water-bottle rocket like propulsion mechanism to generate enough energy to launch a fixed-wing UAV from the water.

Our approach, which also tries to solve both the water-exit and water-entry problem, can be viewed as a hybridization of these two approaches. It maintains the fixed-wing configuration of the latter while utilizing the propulsion mechanism (propeller-driven) of the former. However, our approach is also unique in that it seeks achieve water-exit by exploiting the natural dynamics of the system through trajectory design rather than relying on a novel propulsion design or actuator configuration. While our approach bears some similarity to vertical take-off exploited in [11], our mechanism-free design utilizes automatic control to enable the water-to-air transition and seeks to achieve both efficient aerial and underwater locomotion through wing design.

III. CONCEPTUAL VEHICLE DESIGN

As described above, our vehicle design is largely inspired by the notion that a fixed-wing aerial-aquatic system should be able to exploit its natural dynamics to achieve a more efficient water-to-air transition. Therefore, we do not seek to develop a novel propulsion or actuation mechanism to enable water-exit. Rather, we seek to select the physical parameters of a simple vehicle so as to enable multi-domain locomotion. We start from basic physical arguments, develop simple physical models to explore the design space, and finally test our design using more sophisticated models and trajectory generation approaches.

Throughout this work, we used the maneuver shown in Figure 1 to guide the analysis and design process. This maneuver can be described as follows: In phase one, the vehicle is cruising below the surface of the water. In phase two, the vehicle is rising to the surface. In phase three, the vehicle begins the water-to-air transition, and in phase four, the vehicle executes a prop-hang maneuver. Finally in phase five, the vehicle transitions to forward flight.

A. Propulsion

Using Figure 1 as a guide, it is clear that we will need some manner of propulsion to overcome vehicle drag in both the water and air domains, as well as assist in the water-to-air transition. There are primarily three different types of propulsion modes that have been explored for hybrid aerial-aquatic vehicles: propeller, rocket, and flapping. The authors of [6] made the observation that it would be difficult to construct an actuator with enough energy density to build up large enough speeds under water and achieve a successful (i.e. sustained flight) water-exit. [15] overcomes this issue by leveraging rocket propulsion to enable water-to-air locomotion. [17] shows through simulation that flapping wings with different spatial characteristics can also enable a water-to-air transition.

Our intuition says that an aerial vehicle propeller and electric motor should be able to achieve a successful water-exit, especially if the thrust-to-weight ratio of the the aircraft is much greater than one. Hobbyist foam aircrafts execute this type of "prop-hang" to forward-flight maneuver routinely. If forces related to water-shedding, water tension, and skin-friction drag do not play a significant role, a very light aircraft should be able to escape the water with a propulsion system consisting of an electric motor and propeller used in hobbyist aircraft. The real question with respect to using an aerial propeller is whether or not the same propeller can be used for both water and air propulsion, or if a second propeller will be needed to achieve aquatic locomotion.

As we discovered and also was reported in [14], propellers designed for air can actually be used to achieve reasonably good propulsion underwater as well, and this can be understood from examining the principle of *dynamic similarity*.

The dimensionless parameter that describes propeller thrust is the thrust coefficient, k_T, where propeller thrust is $T = k_T \rho \omega^2 D^4$. Here k_T is a function dependent on the Reynolds number, Re, advance ratio, J, and the Mach number, M, of the propeller blade tip.

To explore dynamic similarity, we are interested in making sure Re, J, and M are equal for the propeller in both water and air.

First, we consider the advance ratio, $J = \frac{U_0}{D\omega}$. This dimensionless parameter will be the same in air and in water so long as the ratio $\frac{U_0}{\omega}$ is constant between the two mediums. We assume that this is possible, given our control over vehicle and propeller speed.

Next, we consider the Reynolds Number. The Reynolds number is a non-dimensional coefficient that allows for the comparison of flows about similar structures in different fluid media [18]. Typically the Reynolds number is written as $Re = \frac{\rho v L}{\mu}$, where ρ is fluid density, v is a characteristic fluid velocity with respect to the object, L is a characteristic dimension, and μ is the dynamic viscosity of the fluid. In general, if the Reynolds number is the same for an object in two different fluids, the two flows are said to be similar.

Consider the Reynolds number for a propeller, which can be written as $Re = \frac{\rho \omega D^2}{\mu}$, where D is the diameter of the propeller and ω is the speed of the propeller. The Reynolds number in air will be $Re_a = \frac{\rho_a \omega_a D^2}{\mu_a}$, and the flow of the Reynolds number in water will be $Re_w = \frac{\rho_w \omega_w D^2}{\mu_w}$, where the subscript a denotes air and the subscript w denotes water. To get similar flows generated by the propeller in both media, we want $Re_a = Re_w$. The speed ratio $\frac{\omega_a}{\omega_w}$ then becomes $\frac{\omega_a}{\omega_w} = \frac{\mu_a \rho_w}{\mu_w \rho_a}$. At 20°C, this approximates to 13.5. Interestingly, this ratio also applies to the fluid flow about the fixed-wing body, $\frac{U_a}{U_w}$, ensuring that if the Reynolds number for the propeller and for the fixed-wing vehicle remain the same in both media, J is guaranteed to be the same as well.

For the Mach number, M, we reason that this dimensionless parameter will have little or no effect on the propeller thrust for the propeller speeds considered in this design. This was verified experimentally by the work in this paper and the work in [14].

To compare the thrust in air and in water when the Reynolds number of the propeller and the vehicle are the same we set

$$k_{T,a} = k_{T,w} \tag{1}$$

$$\frac{T_a}{\rho_a \omega_a^2 D^4} = \frac{T_w}{\rho_w \omega_w^2 D^4} \tag{2}$$

which leads to

$$\frac{T_w}{T_a} = \frac{\rho_w \omega_w^2}{\rho_a \omega_a^2} \approx 4.29. \tag{3}$$

To validate our analysis, we constructed an experimental set-up to measure both propeller thrust in air and in water. Figure 2 shows that our dimensionless analysis matches well with our actual experiments. For water thrust values that are approximately four times the air thrust values, the speed of the propeller is approximately 15 times slower.

1) Propulsive Efficiency: Efficiency can also be expressed in terms of dimensionless coefficients. Propeller efficiency is given as $\eta = \frac{1}{2\pi} \frac{k_T}{k_M} J$. If we assume that k_T and k_M are only dependent on Re and J, then propeller efficiency in water and in air will be equivalent so long as Re for the propeller and the vehicle are also equivalent.

While this dynamic similarity of the propeller and vehicle body across domains is not strictly necessary for our design, it does lead to several convenient features: (1) equivalence of parasitic drag coefficients, (2) equivalent scaling of thrust and drag forces across domains and (3) equivalence of propulsive efficiency. These features allow for vehicle cruise design considerations to be explored in a single domain (e.g., air), and then easily mapped to the other domain (water).

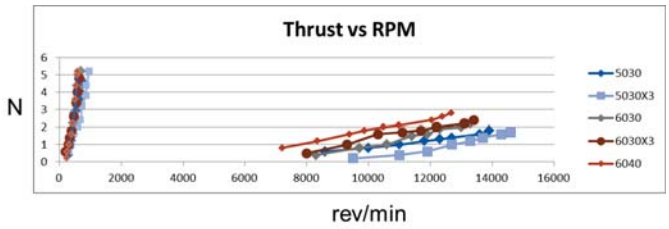

Fig. 2: Thrust vs. angular speed for propeller in water and in air.

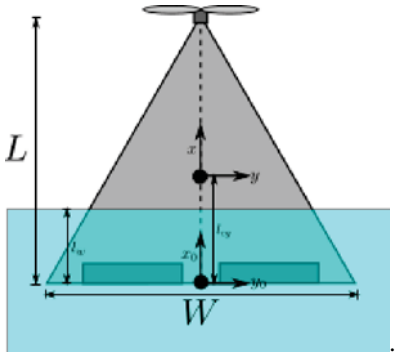

Fig. 3: Diagram of delta-wing planform partially submerged in water.

B. Wing Design

As previously mentioned, there are a number of benefits to fixed-wing vehicles (when compared to rotorcraft). Not only is endurance increased in the air domain, but the existence of lifting surfaces, allows for the design of a vehicle that is positively buoyant (i.e. a negative angle of attack, while the vehicle in motion, will be able to counteract buoyancy forces). This, in turn, leads to a larger design space, where positive buoyancy can be exploited to reduce the propulsive forces required for water exit.

1) Effect of Buoyancy: Our intuition leads us to believe that there will be a non-negligible assist from fuselage/wing buoyancy in the water-to-air transition. We can try to characterize this effect using a simple model. In Figure 3, we show the vehicle during water-exit. Let l be the distance out of the water that vehicle has risen, at some angle θ. The equation of motion along the body of the vehicle can be written as

$$F_b \sin(\theta) - mg \sin(\theta) + F_t = m\ddot{l} \tag{4}$$

where F_b is the buoyancy force, F_t is the applied thrust force. Here F_b is given as $F_b = \rho_w dg A(l)$, leading to

$$\rho_w dg A(l) \sin(\theta) - mg \sin(\theta) + F_t = m\ddot{l}. \tag{5}$$

Integrating and solving for thrust yields

$$F_t = \frac{m}{2L}\left(v_f^2 - v_i^2\right) + mg \sin\theta - \rho_w dg \sin(\theta) \frac{1}{L} \int_0^L A(l) dl. \tag{6}$$

This means that the buoyancy assist, denoted $F_{b,assist}$, for a vehicle with a submerged planform area $A(l)$ is $\rho_w dg \sin(\theta) \frac{1}{L} \int_0^L A(l)dl$, where we denote $\frac{1}{L} \int_0^L A(l)dl$ as the "length-averaged area" (LAA) of our planform. We consider the length-averaged area for three different planforms: semi-elliptical, triangular, and rectangular.

Quantity	Semi-elliptical	Triangular	Rectangular
S	$\frac{1}{2}\pi WL$	$\frac{1}{2}WL$	WL
LAA (WL)	$\approx 0.45WL$	$\frac{1}{3}WL$	$\frac{1}{2}WL$
LAA (S)	$\approx 0.576S$	$\frac{2}{3}S$	$\frac{1}{2}S$

The results summarized in Table III-B.1 show that for a given wing area (i.e, equivalent lifting surface), S, the triangular delta-wing planform maximizes the buoyancy assistance.

IV. VEHICLE DESIGN ANALYSIS

To analyze a candidate vehicle design, we consider the five main phases of the water-exit described in Figure 1. Using these phases, we develop conditions for a successful water exit with closed-form solutions. We consider the trim conditions for the vehicle in swim and prop-hang using a simplified model that ignores the force contributions associated with small control surface deflections. These trim conditions provide the initial and final conditions for the water-exit maneuver, whose physics are governed by Equation 6. The approximate thrust-to-weight ratio required to exit the water with a specific aspect ratio and fuselage density is shown in Figure 4. For this analysis, we used a fixed payload consisting of a motor, electronics and battery (see Section VII-A) with a mass of 200 g and buoyancy of 0.981 N. To limit vehicle size, we restrict ourselves to a 0.6096 m (24 inch) wingspan. While not practical for a final design, we also restrict our airfoil to a flat plate. Their are two reasons for this: aero/hydrodynamic models of flat plates are readily available in the literature and flat plates are simple to manufacture. Finally, we limit ourselves to a maximum thrust-to-weight ratio of one, as a safety factor to account for uncertainty in our analysis.

Given these constraints, our analysis shows that to maximize aspect ratio (and thus maximize vehicle endurance) with the minimum achievable density ratio of 0.3 (based on available materials and minimizing thickness), an aspect ratio of 2.4 should be selected. Our prototype vehicle will have a wing-area of $0.1524m^2$ and a buoyancy assist of $F_{b,assist}$ ≈1.8N at an exit angle of 45°.

In Figure 4, we also plot the thrust-to-weight ratio required for the vehicle to dive straight down at cruise-speed. This provides a lower-bound for maximum wing buoyancy, which could be further explored in future research efforts.

V. VEHICLE MODELING

The prior design analysis used very simplified models to determine thrust required for water-exit. To further investigate the feasibility our design, we develop a higher fidelity dynamic model capable of capturing the physics of the vehicle in and across the air-water domain. We define our state as

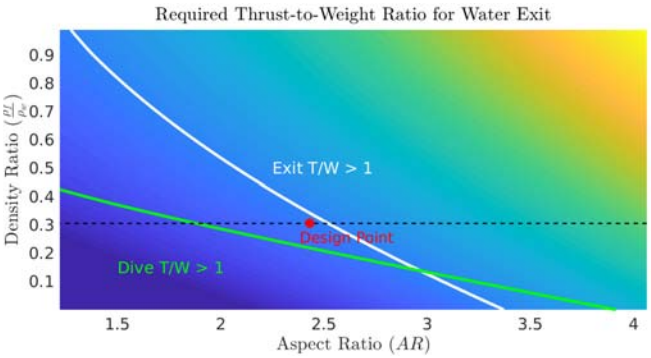

Fig. 4: The effect of fuselage density and aspect-ratio on required water-exit thrust for a vehicle with a 24 inch wingspan. The region to the right of white line exceeds the maximum allowable water-exit thrust and region to the left the green line exceeds the maximum allowable dive thrust. Our design point is represented by the red dot.

$\mathbf{x} = \{r_x, r_y, r_z, \phi, \theta, \psi, \delta_1, \delta_2, v_x, v_y, v_z, \omega_x, \omega_y, \omega_z\}$. Here $\mathbf{r} = \begin{bmatrix} r_x, r_y, r_z \end{bmatrix}^T$ represents the position of the center of mass in the world frame $O_{x_r y_r z_r}$, $\boldsymbol{\theta} = \begin{bmatrix} \phi, \theta, \psi \end{bmatrix}^T$ represents the set of z-y-x Euler angles, $\boldsymbol{\delta} = \begin{bmatrix} \delta_1, \delta_2 \end{bmatrix}^T$ are control surface deflections due to the right and left elevons, $\mathbf{v} = \begin{bmatrix} v_x, v_y, v_z \end{bmatrix}^T$ is the velocity of the center of mass in the *body* fixed frame O_{xyz}, $\boldsymbol{\omega} = \begin{bmatrix} \omega_x, \omega_y, \omega_z \end{bmatrix}^T$ represents the angular velocity of the body the body-fixed frame. We can then write $\mathbf{x} = \{\mathbf{r}^T, \boldsymbol{\theta}^T, \boldsymbol{\delta}^T, \boldsymbol{v}^T, \boldsymbol{\omega}^T\}^T$.

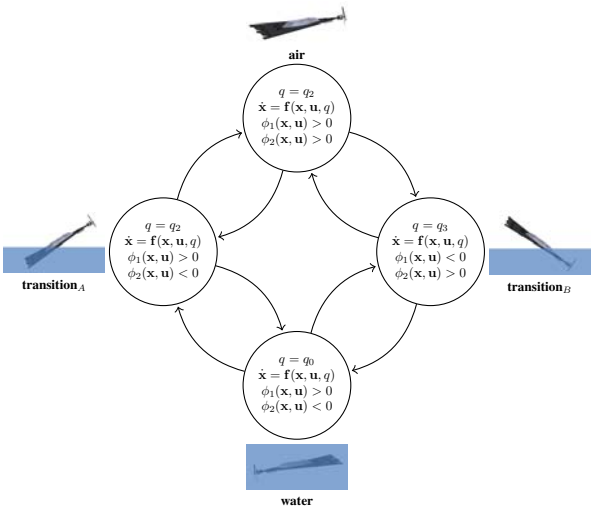

Fig. 5: Depiction of the hybrid dynamical system described by the physics model.

A. Equations of Motion

The equations of motion then become

$$\dot{\mathbf{r}} = \mathbf{R}_b^T \mathbf{v} \tag{7}$$

$$\dot{\boldsymbol{\theta}} = \mathbf{R}_{\boldsymbol{\omega}}^T \boldsymbol{\omega} \tag{8}$$

$$\dot{\boldsymbol{\delta}} = \mathbf{u}_{cs} \tag{9}$$

$$\dot{\boldsymbol{\chi}} = (\mathbf{M} + \mathbf{M}_a)^{-1} \big(\boldsymbol{f} - \boldsymbol{\mathcal{S}}(\boldsymbol{\omega})(\mathbf{M} + \mathbf{M}_a)\boldsymbol{\chi} - \boldsymbol{\mathcal{S}}(\mathbf{v})\mathbf{M}_a \boldsymbol{\chi} \big) \tag{10}$$

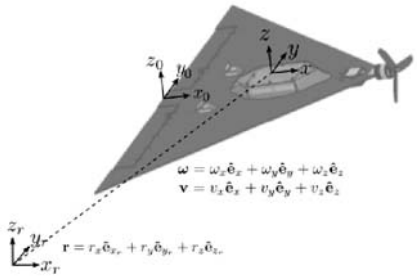

Fig. 6: Diagram depicting the coordinate frames referenced by the dynamic model.

where

$$\boldsymbol{\chi} = \begin{bmatrix}\mathbf{v}, \boldsymbol{\omega}\end{bmatrix}^T, \quad \begin{bmatrix} m\mathbf{I} & \mathbf{0} \\ \mathbf{0} & \mathbf{J} \end{bmatrix}, \quad \boldsymbol{f} = \begin{bmatrix}\mathbf{f}, \mathbf{m}\end{bmatrix}^T \tag{11}$$

$$\boldsymbol{\mathcal{S}}(\boldsymbol{\omega}) = \begin{bmatrix} \mathbf{S}(\boldsymbol{\omega}) & \mathbf{0} \\ \mathbf{0} & \mathbf{S}(\boldsymbol{\omega}) \end{bmatrix}, \quad \boldsymbol{\mathcal{S}}(\mathbf{v}) = \begin{bmatrix} \mathbf{0} & \mathbf{0} \\ \mathbf{S}(\mathbf{v}) & \mathbf{0} \end{bmatrix}. \tag{12}$$

$\mathbf{M}_a$ is the "added mass" matrix m is the vehicle mass, $\mathbf{J}$ is the vehicle's inertia tensor with respect to the center of mass, $\mathbf{f}$ is the total force (excluding the forces due to added mass) applied to the vehicle in body-fixed coordinates, $\mathbf{m}$ are the moments applied about the vehicle's center of mass in body-fixed coordinates, $\mathbf{u}_{cs}$ are the angular velocity inputs of the control surfaces, and

$$\mathbf{S}(\boldsymbol{\omega}) = \begin{bmatrix} 0 & -\omega_z & \omega_y \\ \omega_z & 0 & -\omega_x \\ -\omega_y & \omega_x & 0 \end{bmatrix} \tag{13}$$

$$\mathbf{S}(\mathbf{v}) = \begin{bmatrix} 0 & -v_z & v_y \\ v_z & 0 & -v_x \\ -v_y & v_x & 0 \end{bmatrix}. \tag{14}$$

$\mathbf{R}_b^r$ denotes the rotation from the body-fixed frame to the world frame, and $\mathbf{R}_{\boldsymbol{\omega}}$ is the rotation which maps the euler angle rates to an angular velocity in body-fixed frame.

B. Body Forces

The forces acting on the vehicle can be written as

$$\mathbf{f} = \mathbf{f}_b + \mathbf{f}_f + \mathbf{f}_w + \mathbf{f}_{\delta_1} + \mathbf{f}_{\delta_2}, \tag{15}$$

where $\mathbf{f}_b$ represents the force due to buoyancy, $\mathbf{f}_f$ represents the force due to friction drag, $\mathbf{f}_w$ represents the force due to the wing, and $\mathbf{f}_{\delta_1}$, $\mathbf{f}_{\delta_2}$ represent the forces due to the left and right elevons respectively.

C. Skin Friction Drag Forces

The fuselage skin friction drag,$\mathbf{f}_f$, can be modeled in the body-fixed frame as

$$\mathbf{f}_f = -\frac{v_x^2}{2}(C_{f_A}\rho_A 2S_A + C_{f_F}\rho_F 2S_F)\mathbf{e}_x, \tag{16}$$

where $C_{f_i} = \frac{0.074}{Re_i^{0.2}}$ and $Re_i = \frac{\rho_i U \bar{c}}{\mu_i}$. given by [19, p.356]. Here, S_A and S_F represent the areas of the *aft* and *fore* sections the wing on either side of the waterline. ρ_A and ρ_B are the densities of the fluid wetting the aft and fore sections of the wing, $\bar{c}$ is the mean aerodynamic chord of the wing. Here $i \in \{\mathrm{A}, \mathrm{F}\}$.

D. Buoyancy Forces

The buoyancy forces act along z in the fixed reference frame and can be written as

$$\mathbf{f}_b = \mathbf{f}_{b,w_A} + \mathbf{f}_{b,w_F} + \mathbf{f}_{b,\delta_1} + \mathbf{f}_{b,\delta_2} \tag{17}$$

$$= \mathbf{R}_b^{rT}(f_{b,w_A}\mathbf{e}_{z_r} + f_{b,w_F}\mathbf{e}_{z_r} + f_{b,\delta_1}\mathbf{e}_{z_r} + f_{b,\delta_2}\mathbf{e}_{z_r}). \tag{18}$$

where $f_{b,w_i} = \rho_i S_i dg$ and $f_{b,e_i} = \rho_{\delta_i} S_{e_i} dg$. Here d represents the thickness of the wing/control surface and $g = 9.81 m/s^2$.

E. Wing Forces

To compute the aero- and hydrodynamic forces on the wing, we follow the reasoning of [20]. In these papers, the author develops a relatively accurate means of calculating lift for low-to-moderate aspect ratio delta wings ($AR \in [1, 2]$) up to high angles-of-attack ($\alpha < 30^o$). This was achieved by combining the lift due to potential flow, removing the axial force associated with leading edge suction, and re-incorporating that leading edge suction force as an equivalent "vortex" lift force acting normal to the wing. [20] gives the following equation for calculating the total lift coefficient:

$$C_L = C_{L,p} + C_{L,v}, \tag{19}$$

where $C_{L,p}$ is lift coefficient associated with potential flow and $C_{L,v}$ is lift coefficient associated with the leading edge vortices. Here $C_{L,p}$ is computed following the approach of slender-wing theory presented in [23], [24]. While our vehicle is on the border of being considered a "slender" delta wing, slender-wing theory seems to provide a reasonable overall lift coefficient while only considering the effects of *spanwise* circulation. Considering only *spanwise* circulation allows significant simplifications to be made with respect to center of pressure for the vehicle in a transition (air-water or water-air) mode. [23], [24] find the normal wing force for a slender delta wing to be

$$f_{p,n} = \tag{20}$$
$$\int_0^L \int_{\frac{-w(x_0)}{2}}^{\frac{w(x_0)}{2}} \left(\rho(x_0)|\mathbf{v}|^2 \sin\alpha \frac{w(x_0)}{\sqrt{w(x_0)^2 - 4y_0^2}} \frac{\partial w}{\partial x_0}\right) dy_0 dx_0,$$

where $w(x_0) = \frac{W}{L}(L - x_0)$. As described in Figure 3, W is the width of the delta wing base and L is the length of the delta wing. The coordinate frame $x_0 y_0 z_0$ is positioned at the delta wing base. Carrying out the spanwise integration gives

$$f_{p,n} = \frac{1}{2}|\mathbf{v}|^2 \sin\alpha\pi \frac{\partial w}{\partial x_0}\left(\rho_A \int_0^{l_w} w(x_0)dx_0 + \rho_F \int_{l_w}^{L} w(x_0)dx_0\right). \tag{21}$$

This reduces to

$$f_{p,n} = f_{p,nA} + f_{p,nF} = \frac{1}{2}|\mathbf{v}|^2 C_{n,p}\left(\rho_A S_A + \rho_F S_F\right), \tag{22}$$

where $C_{n,p} = AR\frac{\pi}{2}\sin\alpha$. To compute the component of force on the wing due to the vortex, we use

$$\begin{aligned} f_{v,n} &= f_{v,nA} + f_{v,nF} \\ &= \frac{1}{2}|\mathbf{v}|^2 k_v \sin^2\alpha \int_0^L \rho(x_0) w(x_0) dx_0 \\ &= \frac{1}{2}|\mathbf{v}|^2 k_v \sin^2\alpha \Big(\rho_A S_A + \rho_F S_F\Big) \end{aligned} \tag{23}$$

where $k_v = 2$, as described in [25]. We can then write

$$\begin{aligned} \mathbf{f}_w &= (f_{p,n_A} + f_{v,n_A} + f_{p,n_F} + f_{v,n_F})\mathbf{e}_y \\ &= \mathbf{f}_{w_A} + \mathbf{f}_{w_F}. \end{aligned} \tag{24}$$

For angles of attack greater than 30^o, where vortex breakdown occurs, we revert to a flat plate model [25] of the form

$$f_{fp,n} = f_{fp,n_A} + f_{fp,n_F} = \frac{1}{2}|\mathbf{v}|^2 C_{n,fp}\Big(\rho_A S_A + \rho_F S_F\Big), \tag{25}$$

where $C_{n,fp} = 2\sin\alpha$.

F. Control Surface Forces

To model forces on our control surfaces, we use the flat plate model described above.

$$\mathbf{f}_{\delta_i} = f_{n,\delta_i}\mathbf{e}_y = \frac{1}{2}C_{n,fp}\rho_{\delta_i}|\mathbf{v}_{\delta_i}|^2 S_e \mathbf{e}_y \tag{26}$$

G. Moments

As noted in [24], the potential flow model developed for delta wing lift only considers spanwise circulation, and therefore the center of lift will be at the center of area of the lifting surface. This is evident from an inspection of

$$\begin{aligned} m_p =& \frac{1}{2}|\mathbf{v}|^2 \sin\alpha\pi \frac{\partial w}{\partial x_0}\Big(\rho_A \int_0^{l_w} w(x_0)x_0 dx_0 \\ &+ \rho_F \int_{l_w}^{L} w(x_0)x_0 dx_0\Big) \\ =& \frac{1}{2}|\mathbf{v}|^2 \sin\alpha\pi \frac{\partial w}{\partial x_0}\Big(\rho_A c_A + \rho_F c_F\Big) \end{aligned} \tag{27}$$

and is only possible because $\frac{\partial w}{\partial x_0}$ evaluates to a constant. Here c_A represents the centroid of the aft component of area and c_F the fore in the x_0 direction. A similar observation can be made of the other fluid dynamic forces. $\mathbf{m}$ in the body fixed frame can be given as

$$\begin{aligned} \mathbf{m} =& \sum_{i=A,F}(\mathbf{r}_{w_i} \times \mathbf{f}_{w_i} + \mathbf{r}_{b_i} \times \mathbf{f}_{b_i}) \\ &+ \sum_{i=1,2}(\mathbf{r}_{\delta_i} \times \mathbf{R}_\delta \mathbf{f}_{\delta_i} + \mathbf{r}_{\delta_i} \times \mathbf{f}_{b,\delta_i}) \end{aligned} \tag{28}$$

Here $\mathbf{r}_{w_A} = \mathbf{r}_{b_A} = c_A\mathbf{e}_x$, $\mathbf{r}_{w_F} = \mathbf{l}_{b_F} = c_F\mathbf{e}_x$, and $\mathbf{r}_{\delta_i} = l_h\mathbf{e}_x + \mathbf{R}_\delta(l_\delta \mathbf{e}_{x_\delta})$. $l_h = -l_\delta - l_{cg}$, $c_A = \frac{l_w(2w+L)}{3(w+L)} - l_{cg}$, $c_F = \frac{L-l_w}{3} + l_w - l_{cg}$.

H. Added Mass

The added mass forces are moments are given by the expression $\boldsymbol{f}_a = -\mathbf{M}_a\dot{\boldsymbol{\chi}}$. In [26], the added mass coefficients for a two dimensional flat plate are given as

$$a_{11} = a_{22} = 0 \qquad a_{33} = \pi\rho a^2 \qquad a_{44} = \frac{1}{8}\pi\rho a^4 \tag{29}$$

Where a is the half length of the flat plate, and $1, 2, 3$ represents a coordinate system in the flat plate's body fixed frame. 4 is the rotational dimension. If we once again apply slender body theory, as described in [27], the added mass coefficients in three dimensions for a triangular delta-wing planform are

$$m_{ij} = \pi\rho_A \int_{-l_{cg}}^{l_w - l_{cg}} \mathcal{I}_{ij} dx + \pi\rho_F \int_{l_w - l_{cg}}^{L - l_{cg}} \mathcal{I}_{ij} dx \tag{30}$$

where $\mathcal{I}_{ij} = 0$ except for

$$\mathcal{I}_{33} = a(x)^2 \quad \mathcal{I}_{35} = a(x)^2 x \quad \mathcal{I}_{44} = a(x)^2 x^2 \tag{31}$$

$$\mathcal{I}_{55} = \frac{1}{8}a(x)^4 \quad \mathcal{I}_{53} = -a(x)^2 x. \tag{32}$$

Here $a(x) = w(x)/2$.

I. Densities

The prior sections reference the fore, aft, and control surface densities ρ_A, ρ_F, and ρ_{δ_i} respectively. These densities are a function of the hybrid mode, q, and are defined as

$$\rho_A = \begin{cases} \rho_\mathrm{w} & q \in \{1,2\} \\ \rho_\mathrm{a} & q \in \{3,4\} \end{cases} \quad \rho_F = \begin{cases} \rho_\mathrm{w} & q \in \{1,4\} \\ \rho_\mathrm{a} & q \in \{2,3\} \end{cases} \tag{33}$$

$$\rho_{\delta_i} = \begin{cases} \rho_\mathrm{w} & q \in \{1,2\} \\ \rho_\mathrm{a} & q \in \{3,4\} \end{cases} \tag{34}$$

where $\rho_\mathrm{w} = 1000\frac{kg}{m^3}$ and $\rho_\mathrm{a} = 1.22\frac{kg}{m^3}$.

J. Hybrid Systems Model

To formulate a more well posed non-linear optimization problem, we approximate our vehicle dynamics using a hybrid sate q. We define two guard functions, $\Phi_1(\mathbf{x}, \mathbf{u})$ and $\Phi_2(\mathbf{x}, \mathbf{u})$, which depend of the state of the vehicle's nose and the vehicle's control surface centroids respectively.

$$\Phi_1(\mathbf{x}, \mathbf{u}) = \mathbf{e}_{z_r}^T(\mathbf{r} + \mathbf{R}(L\mathbf{e}_x - l_{cg}\mathbf{e}_x)) \tag{35}$$

$$\Phi_2(\mathbf{x}, \mathbf{u}) = \mathbf{e}_{z_r}^T(\mathbf{r} + \mathbf{R}\mathbf{r}_h + \mathbf{R}\mathbf{R}_\delta(-l_\delta \mathbf{e}_{x_\delta})) \tag{36}$$

For this system the reset map is simply $\mathbf{x} = \Delta(\mathbf{x}, \mathbf{u})$.

VI. TRAJECTORY OPTIMIZATION

To further explore the feasibility of executing a water-to-air transition with the delta-wing vehicle, we attempt to compute an optimal water-exit trajectory. Using the underwater cruise and steady-level flight cruise conditions as the initial and final states, we design an optimal trajectory for our vehicle. To do so, we planarize our dynamic model and only consider the vehicle's *longitudinal* dynamics. For designing a trajectory, we use an approach known as direct collocation. Direct methods are particularly useful since they allow the incorporation of hard constraints on state (and action). This is an important feature and something which can be exploited to generate a trajectory for our aerial-aquatic vehicle.

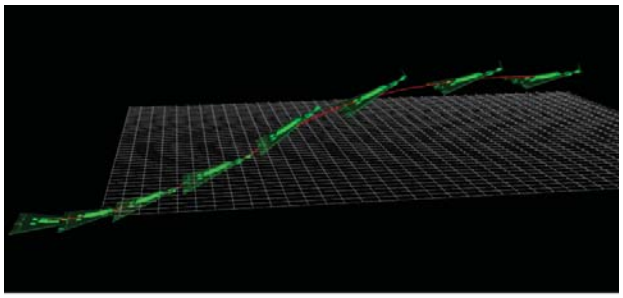

Fig. 7: Optimal water-exit trajectory computed using direct collocation.

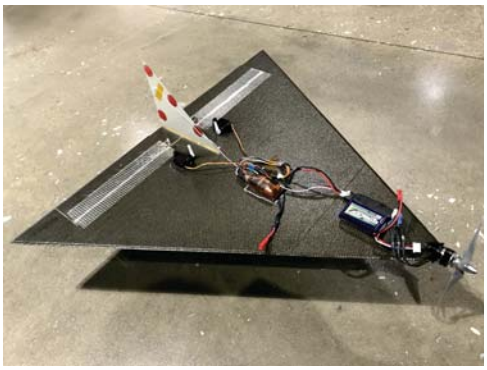

Fig. 8: Photo of our experimental UAAV prototype.

A. Problem Formulation

Assuming a mode schedule, we construct the following optimization problem and let n repesent a discrete set of "sub" time horizons where $N_j = \sum_{i=1}^{j} n_i$, $M_j = N_j - n_j + 1$, $N = N_O + 1$. Our cost-function can be written as

$$\begin{aligned}
\min_{\mathbf{x}_k, \mathbf{u}_k, h_j} \quad & g_f(\mathbf{x}_N) + \sum_{j=1}^{O} \sum_{k=M_j}^{N_j} g(\mathbf{x}_k, \mathbf{u}_k, h_j) \\
\text{s.t.} \quad & \forall k \in \{M_j, \dots N_j\} \text{ and } \forall j \in \{1, \dots O\} \\
& \mathbf{x}_k - \mathbf{x}_{k+1} + \frac{h_j}{6.0}(\dot{\mathbf{x}}_k + 4\dot{\mathbf{x}}_{c,k} + \dot{\mathbf{x}}_{k+1}) = 0 \\
& \Phi_{1,q_j}(\mathbf{x}_k) \geq 0, \quad \Phi_{2,q_j}(\mathbf{x}_k) \geq 0 \\
& \Phi_{e_j,q_j}(\mathbf{x}_{N_j}) = 0 \\
& \mathbf{x}_f - \boldsymbol{\delta}_f \leq \mathbf{x}_N \leq \mathbf{x}_f + \boldsymbol{\delta}_f \\
& \mathbf{x}_i - \boldsymbol{\delta}_i \leq \mathbf{x}_N \leq \mathbf{x}_i + \boldsymbol{\delta}_i \\
& \mathbf{x}_{min} \leq \mathbf{x}_k \leq \mathbf{x}_{max}, \quad \mathbf{u}_{min} \leq \mathbf{u}_k \leq \mathbf{u}_{max} \\
& h_{min} \leq h_j \leq h_{max}
\end{aligned} \tag{37}$$

where

$$\begin{aligned}
& \dot{\mathbf{x}}_k = \mathbf{f}(t, \mathbf{x}_k, \mathbf{u}_k, q_j), \quad \dot{\mathbf{x}}_{k+1} = \mathbf{f}(t, \mathbf{x}_{k+1}, \mathbf{u}_{k+1}, q_j) \\
& \mathbf{u}_{c,k} = (\mathbf{u}_k + \mathbf{u}_{k+1})/2 \\
& \mathbf{x}_{c,k} = (\mathbf{x}_k + \mathbf{x}_{k+1})/2 + h_j(\dot{\mathbf{x}}_k - \dot{\mathbf{x}}_{k+1})/8 \\
& \dot{\mathbf{x}}_{c,k} = \mathbf{f}(t, \mathbf{x}_{c,k}, \mathbf{u}_{c,k}, q_j)
\end{aligned} \tag{38}$$

The cost function can be written as

$$\sum_{j=1}^{O} \sum_{k=M_j}^{N_j} \mathbf{u}_k^T \mathbf{R} \mathbf{u}_k h_j + D h_j. \tag{39}$$

This formulation of the optimization problem allows for trajectory segments to be separated into different modes, while maintaining state continuity across modes and minimizing the control (thrust) effort.

B. Results

The results of our trajectory optimization can be seen in Figure 7. We were able to successfully able to execute the water-exit maneuver without exceeding the thrust limits of our propeller.

VII. EXPERIMENTAL RESULTS

Both our initial analysis and our trajectory optimization have indicated that we should be able to execute a successful water-exit maneuver with the vehicle we have designed. To test the feasibility of executing a water exit maneuver experimentally, we built a prototype vehicle.

A. Vehicle Prototype

Our delta-wing design has an aspect ratio (AR) of 2.4, a wing span of 0.61 m and a center chord length of 0.5 m. The vehicle was constructed using a carbon fiber-foam-carbon fiber sandwich structure. For the core, we used 0.1 inch roahCell 32 IG foam and for the faces we used a single ply of 0.009 inch carbon fiber. A rigid vertical stabilizer constructed from a fiberglass sheet above and below the wing. We selected Hitec HS-5065MG servos to control the elevons and a T-Motor MN1806 KV2300 for propulsion. The servos were waterproofed through the injection of CorrosionX. A Hobbywing FlyFun 18A Brushless ESC sealed with waterproof epoxy was used to drive the motor. To control the vehicle, we used a 72 MHz transmitter and (potted) receiver pair, which was able to provide effective radio control over the vehicle up to depths of around 8 feet. We use a 6 inch APC propeller with a 4 inch pitch.

B. Hand Piloted Testing

To test the ability of our vehicle to execute a successful water-exit, we hand piloted our vehicle through the water-to-air transition. With a highly experienced pilot, we were able to demonstrate several successful water exits, with transitions to forward flight (see Figure 9). From our observations, it is evident that a successful water exit is highly dependent on both body angle at water exit and initial speed. Initial investigations in simulation of the region of attraction for a linear controller applied about the flight trim conditions confirm this. We also tested the vehicle in free flight (see video) and in executing tight turns underwater. With regards to controllability, the vehicle performance was deemed satisfactory.

VIII. CONCLUSION

In this paper, we have demonstrated that it is in fact possible develop a fixed-wing aerial-aquatic vehicle capable

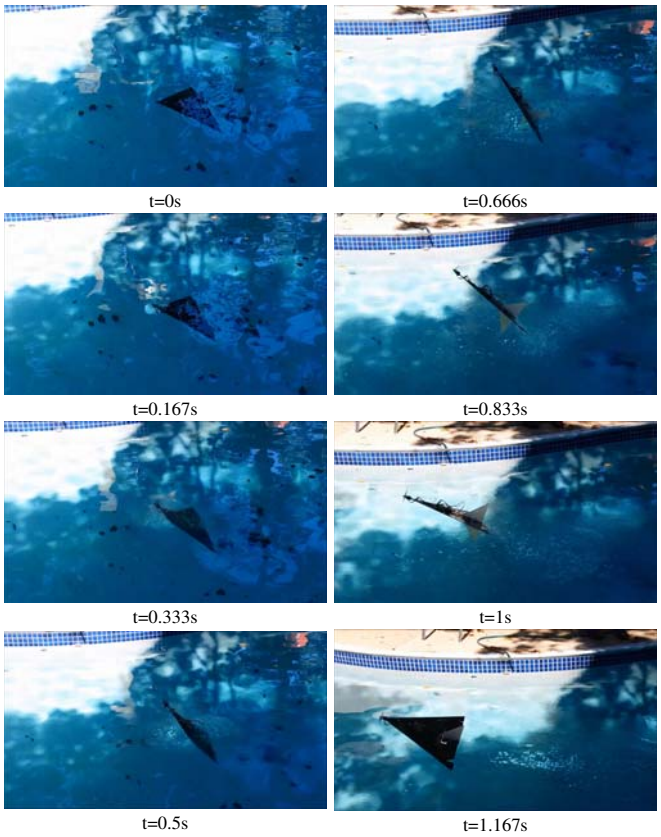

Fig. 9: A time history of the hand-piloted UAAV water-exit maneuver.

of executing a successful water-to-air transition using an electric motor and a single propeller. We have demonstrated that, through the use of positive buoyancy, we can execute a successful water-to-air transition. Because of our lifting surface, not only can we achieve greater endurance compared to quadcopters, we can also tolerate positive buoyancy more effectively. Our future work will focus on achieving closed-loop control for this vehicle. This will undoubtedly require exploring control design strategies, as well as approaches for sensing and state-estimation across the two fluid domains.

One interesting observation which emerges from this paper is that the propeller can operate as both a source of propulsion and a domain transition sensor. Since the motor runs open-loop, when the propeller transitions from water-to-air, the dramatic speed change would likely a robust, low-cost means of sensing the domain change.

ACKNOWLEDGMENT

The authors would like to thank Eddie Tunstel and Robert Osiander for their technical guidance and support through the duration of this project. We would also like to thank Rich Hooks, Galen Mullins, Kevin Wolfe, and the other talented APL staff who have provided valuable ideas and insights. Finally we would like to thank Robert Osiander and Gary Persing for the use of their pools. This project was funded by JHU/APL internal research.

REFERENCES

[1] F. M. Sobolic, "Agile flight control techniques for a fixed-wing aircraft," Ph.D. dissertation, Citeseer, 2009.
[2] X. Yang, T. Wang, J. Liang, G. Yao, and M. Liu, "Survey on the novel hybrid aquatic-aerial amphibious aircraft: Aquatic unmanned aerial vehicle (aquauav)," *Progress in Aerospace Sciences*, vol. 74, pp. 131–151, 2015.
[3] B. D. Reid, *The Flying Submarine: The Story of the Invention of the Reid Flying Submarine, RFS-1*. Eagle Editions, 2004.
[4] G. Pisanich and S. Morris, "Fielding an amphibious uav: development, results, and lessons learned," in *Digital Avionics Systems Conference, 2002. Proceedings. The 21st*, vol. 2. IEEE, 2002, pp. 8C4–8C4.
[5] R. Eubank, E. Atkins, and D. Macy, "Autonomous guidance and control of the flying fish ocean surveillance platform," in *AIAA Infotech@ Aerospace Conference and AIAA Unmanned... Unlimited Conference*, 2009, p. 2021.
[6] A. Gao and A. H. Techet, "Design considerations for a robotic flying fish," in *OCEANS 2011*. IEEE, 2011, pp. 1–8.
[7] A. Fabian, Y. Feng, E. Swartz, D. Thurmer, and R. Wang, "Hybrid aerial underwater vehicle (mit lincoln lab)," 2012.
[8] D. Edwards. (2015) Fying-swimmer (flimmer) uav/uuv. [Online]. Available: https://www.nrl.navy.mil/lasr/content/flying-swimmer-flimmer-uavuuv
[9] Y. Chen, E. F. Helbling, N. Gravish, K. Ma, and R. J. Wood, "Hybrid aerial and aquatic locomotion in an at-scale robotic insect," in *Intelligent Robots and Systems (IROS), 2015 IEEE/RSJ International Conference on*. IEEE, 2015, pp. 331–338.
[10] D. Majumdar, "U.s. navy launches uav from a submarine," 2013. [Online]. Available: https://news.usni.org/2013/12/06/u-s-navy-launches-uav-submarine
[11] R.-A. Peloquin, D. Thibault, and A. L. Desbiens, "Design of a passive vertical takeoff and landing aquatic uav," *IEEE Robotics and Automation Letters*, vol. 2, no. 2, pp. 381–388, 2017.
[12] P. L. Drews, A. A. Neto, and M. F. Campos, "Hybrid unmanned aerial underwater vehicle: Modeling and simulation," in *Intelligent Robots and Systems (IROS 2014), 2014 IEEE/RSJ International Conference on*. IEEE, 2014, pp. 4637–4642.
[13] A. A. Neto, L. A. Mozelli, P. L. Drews, and M. F. Campos, "Attitude control for an hybrid unmanned aerial underwater vehicle: A robust switched strategy with global stability," in *Robotics and Automation (ICRA), 2015 IEEE International Conference on*. IEEE, 2015, pp. 395–400.
[14] M. M. Maia, P. Soni, and F. J. Diez, "Demonstration of an aerial and submersible vehicle capable of flight and underwater navigation with seamless air-water transition," *arXiv preprint arXiv:1507.01932*, 2015.
[15] R. Siddall and M. Kovač, "Launching the aquamav: bioinspired design for aerial–aquatic robotic platforms," *Bioinspiration & biomimetics*, vol. 9, no. 3, p. 031001, 2014.
[16] R. Siddall and M. Kovac, "Fast aquatic escape with a jet thruster," *IEEE/ASME Transactions on Mechatronics*, 2016.
[17] J. S. Izraelevitz and M. S. Triantafyllou, "A novel degree of freedom in flapping wings shows promise for a dual aerial/aquatic vehicle propulsor," in *Robotics and Automation (ICRA), 2015 IEEE International Conference on*. IEEE, 2015, pp. 5830–5837.
[18] F. M. White, "Fluid mechanics,(2003)," *Chap*, vol. 5, p. p287, 2003.
[19] J. D. Anderson Jr, *Fundamentals of aerodynamics - 4th edition*. Tata McGraw-Hill Education, 2010.
[20] E. C. Polhamus, "A concept of the vortex lift of sharp-edge delta wings based on a leading-edge-suction analogy," 1966.
[21] ——, "Application of the leading-edge-suction analogy of vortex lift to the drag due to lift of sharp-edge delta wings," 1968.
[22] ——, "Predictions of vortex-lift characteristics by a leading-edge suctionanalogy," *Journal of aircraft*, vol. 8, no. 4, pp. 193–199, 1971.
[23] E. L. Houghton and P. W. Carpenter, *Aerodynamics for engineering students*. Butterworth-Heinemann, 2003.
[24] J. Katz and A. Plotkin, *Low-speed aerodynamics*. Cambridge university press, 2001, vol. 13.
[25] S. F. Hoerner and H. V. Borst, "Fluid-dynamic lift: practical information on aerodynamic and hydrodynamic lift," 1985.
[26] J. N. Newman, *Marine hydrodynamics*. MIT press, 1977.
[27] E. V. Lewis, "Principles of naval architecture. second revision. volume iii. motions in waves and controllability," *The Society of Naval Architects and Marine Engineers, Jersey City, USA*, 1989.